

Estimation of Ground Motion for Bhuj (26 January 2001; M_w 7.6) and for Future Earthquakes in India

by S. K. Singh, B. K. Bansal, S. N. Bhattacharya, J. F. Pacheco, R. S. Dattatrayam,
M. Ordaz, G. Suresh, Kamal, and S. E. Hough

Abstract Only five moderate and large earthquakes ($M_w \geq 5.7$) in India—three in the Indian shield region and two in the Himalayan arc region—have given rise to multiple strong ground-motion recordings. Near-source data are available for only two of these events. The Bhuj earthquake (M_w 7.6), which occurred in the shield region, gave rise to useful recordings at distances exceeding 550 km. Because of the scarcity of the data, we use the stochastic method to estimate ground motions. We assume that (1) S waves dominate at $R < 100$ km and Lg waves at $R \geq 100$ km, (2) $Q = 508f^{0.48}$ is valid for the Indian shield as well as the Himalayan arc region, (3) the effective duration is given by $fc^{-1} + 0.05R$, where fc is the corner frequency, and R is the hypocentral distance in kilometer, and (4) the acceleration spectra are sharply cut off beyond 35 Hz. We use two finite-source stochastic models. One is an approximate model that reduces to the ω^2 -source model at distances greater than about twice the source dimension. This model has the advantage that the ground motion is controlled by the familiar stress parameter, $\Delta\sigma$. In the other finite-source model, which is more reliable for near-source ground-motion estimation, the high-frequency radiation is controlled by the strength factor, s_{fact} , a quantity that is physically related to the maximum slip rate on the fault. We estimate $\Delta\sigma$ needed to fit the observed A_{max} and V_{max} data of each earthquake (which are mostly in the far field). The corresponding s_{fact} is obtained by requiring that the predicted curves from the two models match each other in the far field up to a distance of about 500 km. The results show: (1) The $\Delta\sigma$ that explains A_{max} data for shield events may be a function of depth, increasing from ~ 50 bars at 10 km to ~ 400 bars at 36 km. The corresponding s_{fact} values range from 1.0–2.0. The $\Delta\sigma$ values for the two Himalayan arc events are 75 and 150 bars ($s_{fact} = 1.0$ and 1.4). (2) The $\Delta\sigma$ required to explain V_{max} data is, roughly, half the corresponding value for A_{max} , while the same s_{fact} explains both sets of data. (3) The available far-field A_{max} and V_{max} data for the Bhuj mainshock are well explained by $\Delta\sigma = 200$ and 100 bars, respectively, or, equivalently, by $s_{fact} = 1.4$. The predicted A_{max} and V_{max} in the epicentral region of this earthquake are 0.80 to 0.95 g and 40 to 55 cm/sec, respectively.

Introduction

The deaths, injuries, and devastation caused by Bhuj earthquake of 26 January 2001 (M_w 7.6) brought sharply into focus the seismic hazard faced by India. The earthquake immediately raised two important questions: (1) What were the ground motions during the Bhuj earthquake, and (2) how can ground motions from future events in India be predicted? The Bhuj earthquake, like the earthquakes of Koyna (1967; M_w 6.3), Latur (1993; M_w 6.1), and Jabalpur (1997; M_w 5.8) occurred in the “stable” Indian shield. North and northeast India, including several mega-cities in the Indo-Gangetic plain, are potentially exposed to much higher seismic hazard

from the large/great earthquakes along the Himalayan arc. It has been suggested that much of the arc may be overdue to rupture in large/great earthquakes (e.g., Bilham *et al.*, 2001). Khattri (1999) has estimated the probability of occurrence of a great M_w 8.5 earthquake in the central seismic gap of the arc (a segment that extends from about 78° E to 85° E) in the next 100 yr to be 0.59.

Estimation of ground motion during the Bhuj earthquake is not straightforward since the closest seismological station, BOM, that recorded the earthquake on-scale was located at a distance of 565 km (Fig. 1). The seismograms at

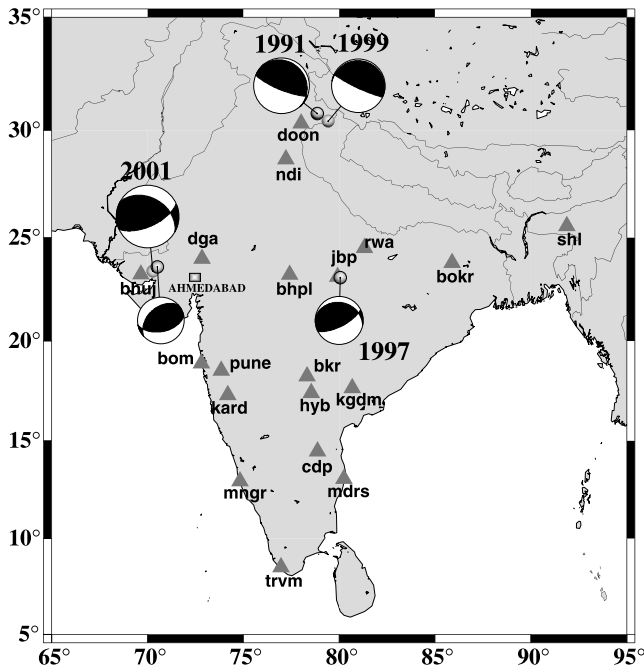


Figure 1. Location of the five earthquakes studied in this article and their focal mechanisms. Triangles indicate BB stations where the Bhuj earthquake of 26 January 2001 (M_w 7.6) was recorded. The recordings at BHUJ and DGA were clipped.

the near-source VBB station of BHUJ and at the BB station DGA ($R \sim 246$ km) were clipped. A peak acceleration of about 100 Gal was recorded on the ground floor of a 10-story building in the city of Ahmedabad, at a distance of about 240 km, but there is some doubt about the performance of the accelerograph. Other digital seismographs and accelerographs recorded the earthquake at distances between 565 and 1795 km (Fig. 2).

The strong motion (SM) data set in India is very sparse. The available free-field SM data of moderate and large ($M_w \geq 5.7$) Indian earthquakes with multiple recordings are summarized in Figure 2. The source parameters of these earthquakes are listed in Table 1. We note that SM recordings within 200 km are available only for two earthquakes, both of which occurred in the central seismic gap of the Himalayan arc (Uttarkashi, 1991, M_w 6.8; Chamoli, 1999, M_w 6.5). The earthquake of Jabalpur (1997, M_w 5.8), like the Bhuj earthquake, was well recorded by VBB seismographs and accelerographs at distances exceeding 500 km but was recorded by only two stations between 240 and 300 km and none at shorter distances (see Singh *et al.*, 1999). The largest aftershock of the Bhuj earthquake (28 January 2001; M_w 5.7) was also recorded at BHUJ at a distance of 100 km. The only earthquake that was well recorded by accelerographs at $R < 250$ km and seismographs at larger distances was the 1999 Chamoli earthquake. Recorded peak accelerations and velocities during the Bhuj mainshock and its aftershock and the Jabalpur and Chamoli earthquakes are listed in Tables 2,

3, 4, and 5, respectively. The values for the Uttarkashi earthquake are given in Yu *et al.* (1995).

In view of the limited SM data available for the Bhuj earthquake in particular, and Indian earthquakes in general, we employ the stochastic method of ground motion prediction (Hanks and McGuire, 1981; Boore, 1983). This approach was followed by Singh *et al.* (1999), who analyzed the Jabalpur earthquake with the goal of predicting ground motions during future earthquakes in the Indian shield region. Using the Jabalpur recordings in the distance range 235 to 1650 km (Fig. 2, Table 4), Singh *et al.* (1999) estimated $Q = 508f^{0.48}$ for L_g waves in the region. They suggested that an ω^2 -source spectrum with stress parameter, $\Delta\sigma$, between 100 and 300 bars, in conjunction with the application of random vibration theory (RVT), might be appropriate to predict the ground motion during future shield earthquakes. Strong motion data from the Chamoli earthquake was analyzed by Singh *et al.* (2002), who found that the Q , as given above, was reasonable for the recordings at a hard-rock site in Delhi.

In this study we will assume that $Q = 508f^{0.48}$ is reasonable for earthquakes in the Indian shield region as well as in the Himalayan arc region. In our application of the stochastic method, we consider two models that account for finiteness of the source. One is an approximate model (Singh *et al.*, 1989), henceforth called the approximate finite-source model, AFSM. The source spectrum in this model reduces in the far field to the point-source ω^2 -spectrum. Hence, the estimated $\Delta\sigma$ values that predict the observed A_{max} and V_{max} in the far field are the same for the AFSM and the point-source model. We find that $\Delta\sigma$ for the Chamoli earthquake, inferred from A_{max} and V_{max} data at $R > 200$ km, also explains the observed data at shorter distances. The $\Delta\sigma$ values estimated from the far-field data from the four earthquakes and near-source data of the Uttarkashi earthquake provide the required, albeit preliminary, estimates of the stress parameter and a measure of its variability. The results may be useful in estimating ground motions during future earthquakes.

Near-source ground motion is very sensitive to the details of the rupture process. We estimate A_{max} and V_{max} values in the near-source region by using a more appropriate source model (Beresnev and Atkinson, 1997, 1998, 1999, 2001), henceforth called the finite source model, FSM. This model requires specification of a “strength factor,” s_{fact} , to explain the high-frequency radiation. We determine the value of s_{fact} by requiring that the predicted curves from FSM and AFSM match each other in the far field up to a distance of about 500 km. For the Bhuj mainshock we present contours of peak ground motions in the near-source region.

A Brief Description of the Stochastic Method

The stochastic method of ground motion prediction was first proposed by Hanks and McGuire (1981) and later ex-

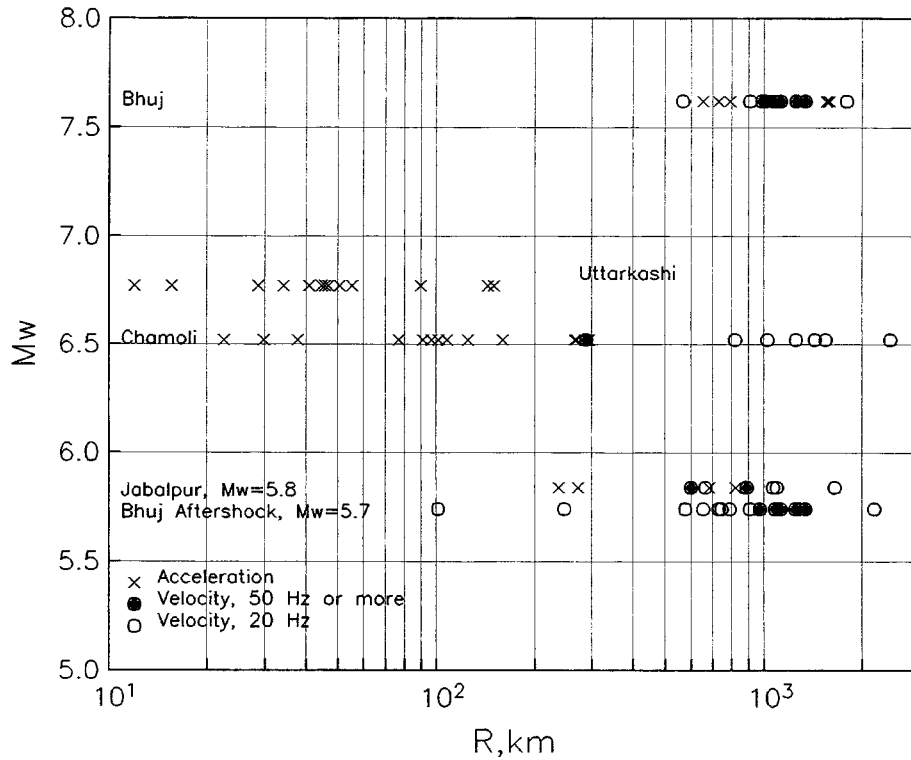


Figure 2. Magnitude, M_w , versus distance from the fault, R , where recordings were obtained. The magnitudes of Jabalpur earthquake and Bhuj aftershock are similar (Table 1); they are plotted at different magnitudes for clarity. Cross, accelerogram; dot and circle, velocity at the sampling rate of 50 and 20 Hz, respectively. Note that near-source ($R < 200$ km) recordings are available only for Chamoli and Uttarkashi earthquakes.

Table 1
Earthquakes and Their Source Parameters

Region	Date	Lat °N	Long °E	Depth, km	M_0 dyne cm	M_w	$\Delta\sigma$, bars ¹		$sfact$ ¹	
							Amax	Vmax	Amax	Vmax
Uttarkashi, Himalayan arc	19 Oct. 1991	30.75*	78.86*	12*	1.8×10^{26}	6.8	75	40	1.0	1.0
Jabalpur, Shield	21 May 1997	23.08 [‡]	80.06 [‡]	36 [§]	5.4×10^{24}	5.8	400	200	2.0	2.0
Chamoli, Himalayan arc	28 Mar. 1999	30.41*	79.42*	21*	7.7×10^{25}	6.5	150	150	1.4	1.7
Bhuj, Mainshock, Shield	26 Jan. 2001	23.41*	70.18*	20 [†]	3.4×10^{27}	7.6	200	100	1.4	1.4
Bhuj, Aftershock, Shield	28 Jan. 2001	23.61*	70.46*	15 [†]	5.2×10^{24}	5.7	50	35	1.0	1.0

*India Meteorological Department

[†]Harvard CMT catalog

[‡]Bhattacharya *et al.* (1997)

[§]Singh *et al.* (1997)

¹Stress drop, $\Delta\sigma$, is the parameter required to fit the observed peak ground motions data (Amax or Vmax) in the far field. Strength factor, $sfact$, is estimated by requiring that the predictions from the approximate finite source and the finite source models equal in the far field at $R < 500$ km.

tended by Boore (1983). Hanks and McGuire (1981) related root mean square (rms) acceleration to an ω^2 -source spectrum modified by attenuation, through Parseval's theorem. The expected peak amplitude is obtained from the rms amplitude and the estimated duration of the strong ground motion (T_R) using equations of random vibration theory (Cartwright and Longuet-Higgins, 1956). Boore (1983) extended these results to predict Vmax and response spectra. Here, we

briefly outline some relevant aspects of the method as used in this study.

The far-field Fourier acceleration spectral amplitude of the strongest ground motions at a distance R from the source, $A(f, R)$, can be written as

$$A(f, R) = C \times S(f) \times G(R) \times e^{-\pi f R / \beta Q(f)}, \quad (1)$$

where,

Table 2
Peak Velocities, Vmax, and Accelerations, Amax, During the 26 January 2001 Bhuj Mainshock

Distance R (km)	Vmax (cm/sec)			Amax (Gal)			Station
	N	E	Z	N	E	Z	
246	Clipped	>1.57, Clipped	Clipped	—	—	—	DGA*
565	1.147	1.171	0.985	4.95	4.47	2.87	BOM*
654	0.964	1.306	1.114	2.808	3.68	2.434	PUNE†
730	1.030	0.949	1.035	3.540	2.116	1.498	BHPL‡
757	1.494	1.61	1.55	2.64	2.68	1.51	DOON*
789	1.010	1.139	1.048	1.508	2.030	1.498	KARD‡
908	1.176	1.250	1.08	2.16	2.53	1.41	NDI*
986	0.571	0.555	0.600	1.57	0.973	1.207	JBP§
1010	0.874	0.528	0.857	1.87	1.66	0.822	BKR ^l
1070	>0.63 (clipped)	0.52	>0.63 (clipped)	—	2.11	—	HYB [#]
1122	0.703	0.636	0.636	1.69	1.11	1.757	REWA§
1252	0.748	0.598	0.724	2.15	2.70	2.75	KGDM ^l
1255	0.366	0.437	0.569	0.66	1.19	0.49	MNGR*
1338	0.660	0.693	0.667	1.936	1.606	1.035	CDP ^l
1552	0.708	0.600	0.530	1.337	1.290	0.6906	MDRS**
1585	0.949	0.957	1.022	1.316	0.895	0.492	BOKR ^{†‡}
1794	0.388	0.420	0.420	0.28	0.63	0.31	TRVM [†]

*Velocity from RefTek (24-bit) digitizer + CMG40T, sampling rate 20 Hz, acceleration from differentiation.

†Velocity from Quanterra (24-bit) digitizer + STS-2, sampling rate 20 Hz, acceleration from differentiation.

‡Acceleration from Quanterra (24-bit) digitizer + FBA-23, sampling rate 80 Hz, velocity from integration.

§Velocity from RefTek (24-bit) digitizer + CMG40T, sampling rate 50 Hz, acceleration from differentiation.

^lVelocity from RefTek (24-bit) digitizer + CMG40T, sampling rate 100 Hz, acceleration from differentiation.

[#]Velocity from RefTek (24-bit) digitizer + CMG 3ESP, sampling rate 200 Hz, acceleration from differentiation.

**Velocity from Quanterra (24-bit) digitizer + STS-2, sampling rate 20 Hz and acceleration from Quanterra (24-bit) digitizer + FBA-23, sampling rate 20 Hz.

Table 3
Peak Velocities, Vmax, and Accelerations, Amax, During the 28 January 2001 Bhuj Aftershock

Distance R (km)	Vmax (cm/sec)			Amax (Gal)			Station
	N	E	Z	N	E	Z	
101	0.569	0.367	0.328	7.32	7.71	4.13	BHUJ*
249	0.191	0.058	0.079	1.671	1.267	1.114	DGA [†]
576	0.038	0.032	0.025	0.261	0.229	0.188	BOM [†]
654	0.020	0.025	0.022	0.109	0.140	0.151	PUNE*
730	0.039	0.014	0.018	0.200	0.122	0.089	BHPL*
744	0.027	0.027	0.017	0.118	0.147	0.055	DOON [†]
789	—	0.020	0.013	—	0.083	0.078	KARD*
907	0.018	0.018	0.014	0.106	0.079	0.046	NDI [†]
970	0.018	0.011	0.009	0.057	0.045	0.054	JBP‡
1082	0.014	0.012	0.012	0.076	0.054	0.047	HYB§
1122	0.015	0.007	0.011	0.080	0.050	0.068	REWA‡
1246	0.022	0.014	0.021	0.129	0.098	0.093	KGDM ⁵
1276	0.008	0.012	0.006	0.051	0.054	0.027	MNGR [†]
1339	0.020	0.017	0.008	0.075	0.063	0.050	CDP ^l
2178	0.004	0.002	0.003	0.009	0.008	0.005	SHL [†]

*Velocity from Quanterra (24-bit) digitizer + STS-2, sampling rate 20 Hz, acceleration from differentiation.

†Velocity from RefTek (24-bit) digitizer + CMG40T, sampling rate 20 Hz, acceleration from differentiation.

‡Velocity from RefTek (24-bit) digitizer + CMG40T, sampling rate 50 Hz, acceleration from differentiation.

§Velocity from RefTek (24-bit) digitizer + CMG 3ESP, sampling rate 200 Hz, acceleration from differentiation.

^lVelocity from RefTek (24-bit) digitizer + CMG40T, sampling rate 100 Hz, acceleration from differentiation.

Table 4
Peak Accelerations, Amax, and Velocities, Vmax, During the 1997 Jabalpur Earthquake

Distance R (km)	Amax (Gal)			Vmax (cm/sec)			Station
	N	E	Z	N	E	Z	
237	12.3	11.4	4.10	0.479	0.465	0.268	BLSP*
271	5.9	8.4	4.7	0.180	0.247	0.152	BHPL [†]
600	0.693	0.887	0.345	0.077	0.084	0.038	BOKR [‡]
665	0.59	0.56	0.470	0.062	0.064	0.039	AJMR [§]
684	0.604	0.541	0.496	0.039	0.057	0.086	VISK [†]
820	0.253	0.192	0.172	0.025	0.027	0.023	PUNE [†]
886	0.271	0.219	0.232	0.025	0.031	0.029	KARD [†]
1066	0.089	0.089	0.068	0.012	0.015	0.012	BHUI [§]
1108	—	—	—	0.014	0.023	0.009	MDRS [§]
1646	0.078	0.107	0.051	0.013	0.016	0.021	TRVM [§]

*Velocity from Quanterra (24-bit) digitizer + STS-2, sampling rate 20 Hz, acceleration from Quanterra (24-bit) digitizer + FBA-23, sampling rate 80 Hz.
[†]Velocity from Quanterra (24-bit) digitizer + STS-2, sampling rate 80 Hz, acceleration from Quanterra (24-bit) digitizer + FBA-23, sampling rate 80 Hz.
[‡]Velocity from Quanterra (24-bit) digitizer + STS-2, sampling rate 80 Hz, acceleration from integration.
[§]Velocity from Quanterra (24-bit) digitizer + STS-2, sampling rate 20 Hz, acceleration from integration.
[†]Acceleration from Quanterra (24-bit) digitizer + FBA-23, sampling rate 80 Hz, velocity from Quanterra (24-bit) digitizer + STS-2, sampling rate 20 Hz.

Table 5
Peak Accelerations, Amax, and Velocities, Vmax, During the 1999 Chamoli Earthquake (Modified from Singh *et al.*, 2002)

Distance R (km)	Amax (Gal)			Vmax (cm/sec)			Station
	H1	H2	Z	H1	H2	Z	
23	199.0	359.0	156.0	22.55	45.30	7.50	Gopeshwar*
30	71.0	63.0	41.00	3.180	8.940	2.72	Joshimath*
38	91.0	96.0	47.00	6.850	5.450	4.05	Ukhimath*
77	73.0	83.0	39.0	3.310	4.080	2.00	Ghansial*
91	54.0	62.0	34.0	4.600	5.380	2.11	Tehri*
97	27.0	28.0	27.0	2.350	1.893	1.270	Almora*
97	5.0	6.0	11.0	0.175	0.214	0.248	Lansdowne*
102	54.0	64.0	23.0	3.550	4.670	1.580	Uttarkashi*
108	52.0	45.0	49.0	3.120	3.300	3.140	Chinyalisaut*
126	17.0	23.0	19.0	0.830	1.240	0.766	Barkot*
160	56.0	47.0	17.0	—	—	—	Roorkee*
265	45.61	28.0	9.43	—	—	—	Panipat*
268	13.5	—	8.23	—	—	—	Baghpat*
292	10.92	8.86	5.78	1.299	0.690	0.546	CSIR, Delhi [†]
287	11.55	14.32	5.59	2.010	1.645	0.634	CPCB, Delhi [†]
293	9.67	11.41	8.23	1.745	1.240	0.673	IHC, Delhi [†]
288	2.69	3.30	2.29	0.617	0.978	0.394	Ridge Obs., Delhi [‡]
819	0.188	0.440	0.410	0.069	0.173	0.173	BHPL [§]
1026	0.220	0.340	0.200	0.140	0.094	0.098	Nagpur [§]
1251	0.210	0.180	0.180	0.100	0.088	0.110	BHUI [§]
1431	0.110	0.240	0.170	0.075	0.110	0.140	PUNE [§]
1545	0.100	0.220	0.120	0.075	0.076	0.096	KARD [§]
2437	0.071	0.130	0.092	0.048	0.059	0.060	TRVM [§]

*Accelerograph, data available at 50 sps. H1 and H2 at these stations refer to the two horizontal components; for other stations they refer to NS and EW components. Velocity from integration.
[†]Accelerograph, data available at 200 sps. Velocity from integration.
[‡]Seismograph (RefTek 24-bit digitizer connected to 1-s natural period L-4C-3D seismometer), data available at 50 sps. Acceleration by differentiation.
[§]Seismograph (Quanterra 24-bit digitizer connected to STS-2 seismometer), data available at 20 sps. Acceleration by differentiation.

$$C = F \times P \times R_{\theta\phi} \times (2\pi)^2 / (4\pi\rho\beta^3), \quad (2)$$

F is the free surface amplification; *P* takes into account the partitioning of energy in the two horizontal components; *R*_{θφ} is the average radiation pattern; ρ, is density; and β is shear-

wave velocity. In this study we will assume *F* = 2.0, *P* = 1/√2, *R*_{θφ} = 0.55, ρ = 2.85 gm/cm³, and β = 3.6 km/sec. *S*(*f*), the source acceleration spectrum, may be written as

$$S(f) = f^2 \dot{M}_0(f), \quad (3)$$

where $\dot{M}_0(f)$ is the moment-rate spectrum. For a ω^2 -source model,

$$S(f) = f^2 f_c^2 M_0 / (f^2 + f_c^2), \quad (4)$$

where M_0 is the scalar seismic moment. For Brune's source model (Brune, 1970), f_c the corner frequency, is given by

$$f_c = 4.9 \times 10^6 \times \beta \times (\Delta\sigma/M_0)^{1/3}, \quad (5)$$

where β is in km/sec, M_0 is in dyne cm, and $\Delta\sigma$, the stress drop, is in bars.

The geometrical spreading term in equation (1), $G(R)$, may be taken as $G(R) = R^{-1}$ for $R \leq R_x$ and $G(R) = (RR_x)^{-1/2}$ for $R > R_x$. This form of $G(R)$ implies dominance of body waves for $R \leq R_x$ and of Lg and surface waves for $R > R_x$. Herrman and Kijko (1983) show that R_x is roughly twice the crustal thickness. In this study, we will take $R_x = 100$ km.

As mentioned above, we will assume that $Q(f) = 508f^{0.48}$ (Singh *et al.*, 1999) is valid for all earthquakes studied here. Since the form of $G(R)$ assumed by Singh *et al.* in the estimation of $Q(f)$ was the same as above, their result is directly applicable to the present study.

In this study our goal is to estimate ground motions on "hard sites." Even at such sites the seismic motions are amplified at high frequencies due to the presence of thin weathered layers. We will assume that this amplification is cancelled by the near-surface attenuation such that the net effect is 1 for $f \leq f_m$. Beyond f_m , the observed acceleration spectra drop off. This has been attributed to the attenuation caused by near-surface materials (Hanks, 1982; Singh *et al.*, 1982; Anderson and Hough, 1984) or to the source processes (e.g., Papageorgiou and Aki, 1983). It may also result from the sampling rate of the recordings. To simulate the observed high-frequency fall off of the spectra, we multiply the right-hand side of equation (1) by a Butterworth filter given by $[1 + (ff_m)^8]^{-1/2}$ (Boore, 1983). The sampling rate of the many seismograms obtained at $R > 250$ km is 20 Hz (Fig. 2), in which case, f_m should be set at about 8 Hz or so. However, as will be shown later, the computed Amax and Vmax are not sensitive to these choices of f_m at $R > 250$ km. At shorter distances, however, the peak values, especially Amax, are sensitive to the choice of f_m . We note that there is a lack of knowledge on f_m in the Indian shield region. In our calculations we have set f_m to 35 Hz. There may be a geological and wave-propagation similarity between the Indian shield region and the eastern North America (ENA). For estimating ground motions in the ENA, Atkinson and Boore (1995) assume $f_m = 50$ Hz. As shown later, there is little difference in the predicted peak ground motions corresponding to $f_m = 35$ and 50 Hz.

Following Herrmann (1985), the effective duration of the ground motion, T_R , is taken as $T_R = f_c^{-1} + 0.05R$, where f_c is the corner frequency (equation 5) and R is the hypocentral distance in km.

As mentioned previously, the seismic-wave propagation in the Indian shield region and ENA may be similar. There is ample literature on the application of stochastic method for ground motion estimation in ENA. A review of the literature is given by Atkinson and Boore (1998). Over the years, the parameters used in the application of stochastic method to ground motion estimation in ENA have evolved. In the most recent version, Atkinson and Boore (1995) choose a source spectrum defined by two corner frequencies. They also use a complicated functional form of the geometrical spreading, $G(R)$, and effective duration, T_R . In this article we opt for the parameters given above. The available data in India do not justify a more complicated choice of these parameters.

Extension to Finite Source

The previous formulation is valid if the far-field approximation (i.e., the source dimension and the wavelength of interest are smaller than the distance to the observation) holds. For moderate and large earthquakes, the approximation breaks down at near-source distances, at which the finiteness of the source must be taken into account. We consider two models that account for the source finiteness. In the AFSM, the fault area (assumed to be circular) is divided into small elements that rupture randomly with uniform probability over the source duration (Singh *et al.*, 1989). In this model, the expression for the Fourier spectrum of ground motion at distances much greater than the radius of the fault reduces to that of the ω^2 -source model. Figure 3 shows computed Amax and Vmax as a function of the closest distance to the fault, R , for the AFSM and as a function of hypocentral distance for a point source model. The computations have been made for the stress parameter, $\Delta\sigma$, of 150 bars. We note that Amax and Vmax predicted by the two models differ for $(r_0/R) > 1$, where r_0 , the radius of the fault, is related to the corner frequency f_c , for the Brune model, by $r_0 = 0.372\beta/f_c$ (Brune, 1970). The estimated r_0 for M_w 7.6, 6.5, and 5.7 with $\Delta\sigma = 150$ bars is 21.0, 5.9, and 2.4 km, respectively. For $(r_0/R) < 1$, the predicted values from the two models are the same. Also, the saturation of near-source Amax and Vmax values with magnitude, predicted by the AFSM, agrees with observations. These features, however, should not be construed as proof of the adequacy of this approximate model in predicting near-source ground motion. For example, the model is approximate at frequencies smaller than the corner frequency and does not allow for source directivity. Nevertheless, the model provides a rough estimate of near-source ground motion and at the same time, reduces to point-source ω^2 -model in the far field. We recall that much of the data in India are available in the far field. We will use the AFSM to estimate the $\Delta\sigma$ values that explain the recorded data.

The second finite-source stochastic model, FSM, that we explore aims to provide a more accurate estimation of near-source ground motions (Beresnev and Atkinson, 1997, 1998,

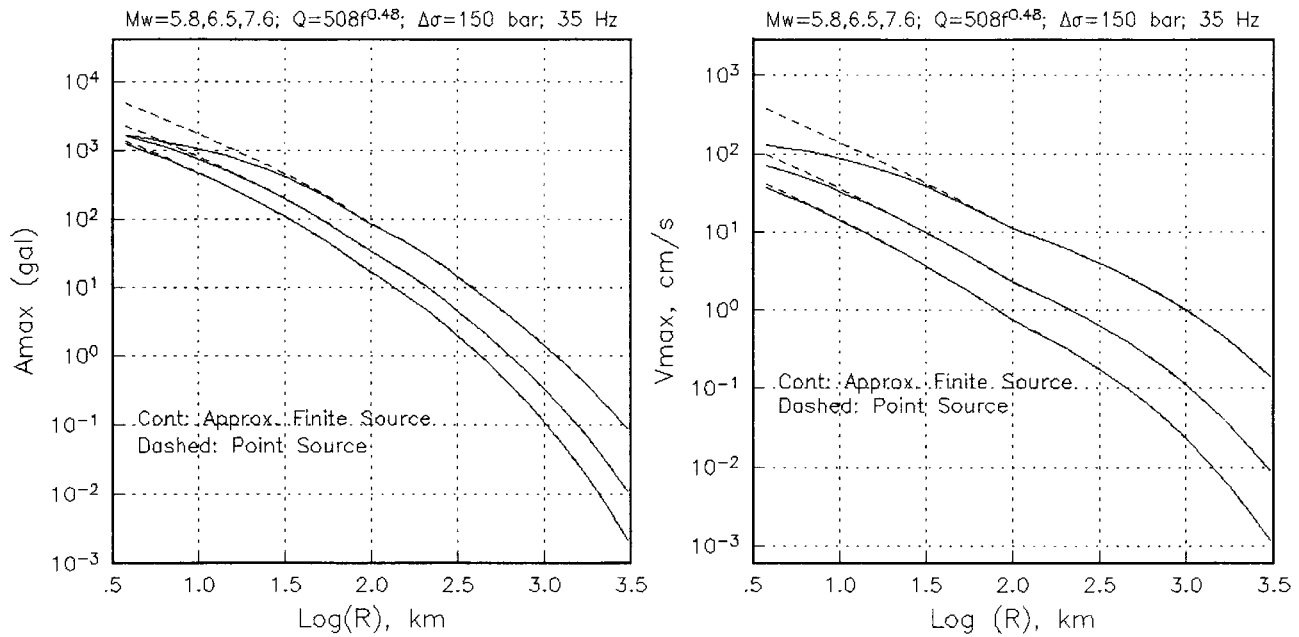


Figure 3. Predicted A_{max} and V_{max} curves as function of R for M_w 5.8, 6.5, and 7.6 for point-source (dashed) and approximate finite-source models (continuous). In this and succeeding figures, R is the hypocentral distance for the point source model and the minimum distance to the fault for the finite source model. $Q = 508f^{0.48}$, $\Delta\sigma = 150$ bars, $f_m = 35$ Hz. Note that for M_w 7.6, the curves corresponding to point source and finite source are indistinguishable for $R > 35$ km; for smaller M_w this distance is smaller.

1999, 2001). In the FSM, the fault plane is divided in subfaults whose preferred size, Δl , in km, is given by $\log \Delta l = 0.4M_w - 2.0$ (Beresnev and Atkinson, 1999). In some cases this results in less than 16 subfaults. If so, we decrease Δl so that the number becomes 16. This ensures realistic shape of accelerograms. Each subfault is a stochastic ω^2 source. The subfault time history at a site is generated following the procedure of Boore (1983). The rupture propagates radially from a specified hypocenter. A standard technique sums the contribution from each subfault. Randomness is introduced in the subfault rupture times. The stress parameter that relates seismic moment of the subfault and its size is fixed at 50 bars. A free parameter, called the strength factor, s_{fact} , which controls the level of high-frequency radiation, needs to be specified (see Beresnev and Atkinson, 1997, 1998). This factor is related to maximum slip rate, v_m , on the fault by (Beresnev and Atkinson, 2002)

$$v_m = 0.618 (V_R/\beta) (\Delta\sigma) (s_{fact})/(\rho\beta), \quad (6)$$

where, V_R is the rupture velocity. In the simulation, V_R/β is taken as 0.8. For simplicity, we present the results in terms of s_{fact} . Equation (5) permits calculation of the corresponding physical parameter v_m . The slips on the subfaults are assigned normally distributed random values with both the mean and the standard deviation equal the average slip. If the slip on a subfault turns out to be negative, its value is taken as zero. The average slip on the fault, Δu , is obtained

from the relation $M_0 = \mu A \Delta u$, where μ is the rigidity and A is the fault area. Alternatively, the slip may be prescribed if it is known from source inversion. All other required parameters are the same as in the previous model. We emphasize that the source spectrum of the entire event does not follow the ω^2 model. A description of the computer program is given in Beresnev and Atkinson (1998). We use this model to synthesize ground motions from all earthquakes listed in Table 1.

The shapes of the attenuation curves computed from AFSM and FSM are expected to differ at near-source distances. They also differ in the far field at large distances. This is because the source spectrum in the far field deviates from ω^2 in the FSM but not in the AFSM. The FSM source spectra show ‘‘sag’’ at low frequencies. Tests show that in our case this sag does not affect the peak values in the far field, at distances $R < 500$ km. The shapes of the attenuation curves obtained from the AFTSM and the FSM are the same in this distance range. At long distances ($R > 500$ km), the anelastic attenuation diminishes high-frequency amplitudes. In this case, the peak ground motions are controlled by relatively low frequencies. Since at these frequencies the source spectra of FSM and ATSM differ, so also do the attenuation curves. For this reason, in our application of the FSM we search for s_{fact} by requiring that the far-field predictions of FSM agree with the predictions of AFSM up to a distance of about 500 km. This ensures that our predictions for $R < 500$

km, based on FSM, roughly corresponds to ω^2 -source model in the far field.

Sensitivity Study

Boore and Atkinson (1987) present a detailed analysis of the sensitivity of the results obtained from the application of the stochastic method to the choice of different parameters. Among the parameters that control the ground motion, the high-frequency cutoff of the spectrum and the quality factor, Q , are two of the more important ones in the present study. Subsequently we discuss the sensitivity of the results to our choice of these parameters. The tests are based on computations using the AFSM.

Sampling Rate and High-Frequency Cutoff of the Spectrum

As mentioned previously and seen in Figure 2 and Tables 2 to 5, many recordings at $R > 500$ km, and some in the distance range of 235–500 km, are available at a sampling rate of 20 Hz. For closer recordings ($R < 230$ km), the sampling rate is 50 Hz or higher, with the exception of the aftershock recording of the Bhuj earthquake at BHUJ, which is at 20 Hz. This suggests that in our analysis, f_m should be set to about 8 Hz at $R > 230$ km and at a higher frequency at closer distances. Figure 4 compares predicted values with $f_m = 8, 35, 50,$ and 100 Hz. We note that the A_{max} and V_{max} values are insensitive to the choice of f_m for $R > 300$ and 200 km, respectively. As expected, at closer distances

the peak ground motions, especially A_{max} , are much greater for $f_m \geq 35$ Hz compared with the values for $f_m = 8$ Hz. Note, however, that the predicted A_{max} values corresponding to $f_m = 35, 50,$ and 100 Hz differ by less than 40%. We will arbitrarily set $f_m = 35$ Hz in our calculations. Unless f_m is much greater than 35 Hz, we expect little error from this assumption.

Broadband velocity recordings are available at sampling rates that vary between 20 and 200 Hz. The sampling rate of acceleration traces, recorded by Quanterra digitizers, is at 20 or 80 Hz. We have differentiated the velocity traces to get accelerations and integrated the acceleration traces to obtain velocities. The values listed in the tables have been obtained from the velocity or the acceleration trace, depending upon which is available at the highest sampling rate.

Q-Value

The prediction of ground motion at close distances is less affected by uncertainty in Q than at far distances. Since the bulk of our data comes from $R > 500$ km, the values of $\Delta\sigma$ and s_{fact} required to fit these data depend on Q . The $\Delta\sigma$ and s_{fact} would, in turn, affect estimates of A_{max} and V_{max} at near-source distances. In Figure 5 we compare predictions of A_{max} and V_{max} based on $Q = 508f^{0.48}$, estimated from Jabalpur data, and the $Q = 680f^{0.36}$, reported by Atkinson and Boore (1995) for ENA. The curves in the top frames correspond to $\Delta\sigma = 150$ bars. The predicted A_{max} and V_{max} are identical for $R < 300$ km but, as expected, are sensitive to Q at larger distances. In the bottom two frames

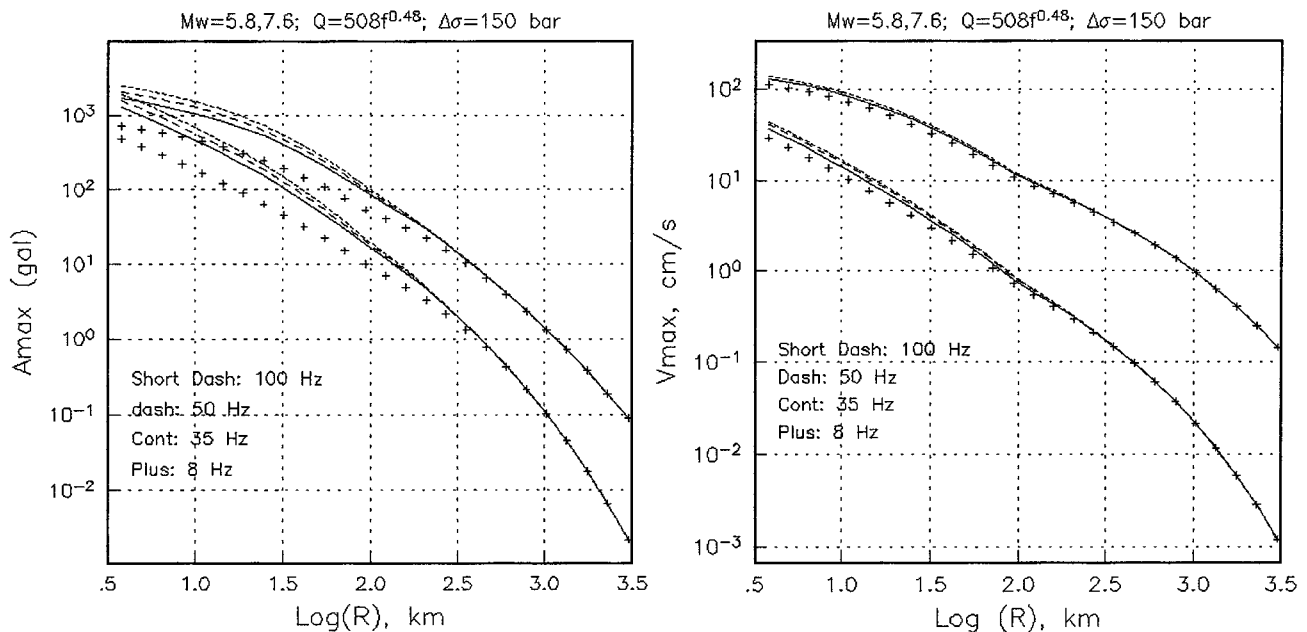


Figure 4. Same as Figure 3 for approximate finite-source model, with $f_m = 8$ Hz, 35 Hz, 50 Hz, and 100 Hz. The predicted V_{max} and A_{max} at R greater than 100 and 320 km, respectively, are not sensitive to the choice of f_m .

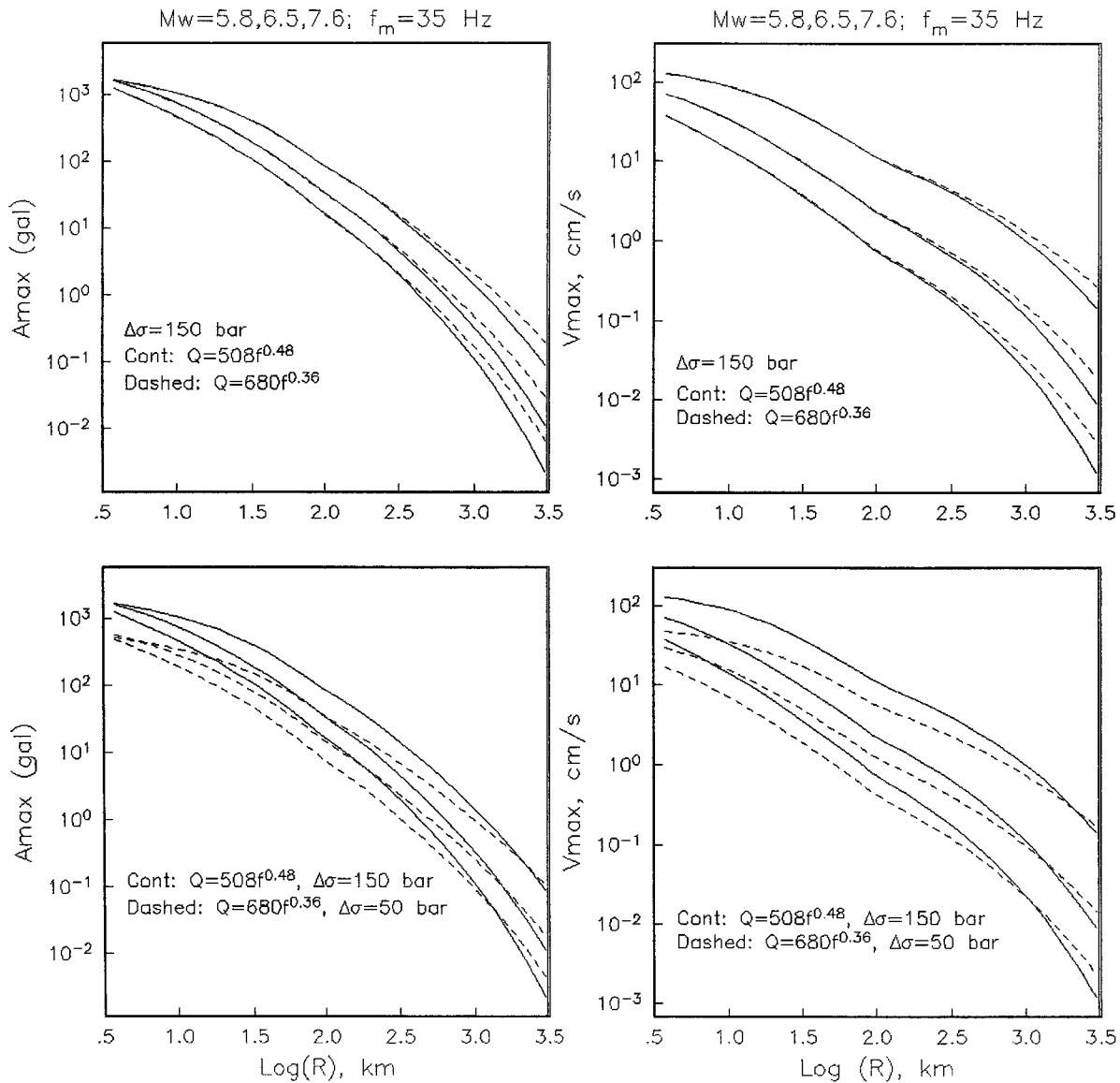


Figure 5. Predicted Amax and Vmax for approximate finite-source model, $f_m = 35$ Hz, and $Q = 508f^{0.48}$ (continuous curves) and $680f^{0.36}$ (dashed curves). Top frames: $\Delta\sigma = 150$ bars. Note that the predicted values at $R > 300$ km are sensitive to Q . Bottom frames: $Q = 508f^{0.48}$ and $\Delta\sigma = 150$ bars (continuous curves); $Q = 680f^{0.36}$ and $\Delta\sigma = 50$ (dashed curves). The predictions are similar around $R = 1000$ km but differ by a factor of about two in the near-source region.

of Figure 5, the predicted peak ground motions with $Q = 508f^{0.48}$ and $\Delta\sigma = 150$ bars are compared with those with $Q = 680f^{0.36}$ and $\Delta\sigma = 50$ bars. The predictions are similar around $R = 1000$ km. Thus, if observed data are mostly from this distance range (as is the case in the present study), then the choice of $Q = 508f^{0.48}$, when the true attenuation is given by $Q = 680f^{0.36}$, will require larger $\Delta\sigma$ to fit the data and, hence, would predict a factor of two larger peak ground motions in the near-source region. It appears that the uncertainty in the Q structure in India could easily lead to an uncertainty of factor of two in predicted peak values at close distances.

Estimation Stress Parameter and Strength Factor from the Recorded Data

We now consider individual earthquakes listed in Table 1 and estimate the values of $\Delta\sigma$ and s_{fact} , required to explain the observed data. We repeat that the calculations assume $R_x = 100$ km, $Q = 508f^{0.48}$, $T_R = f_c^{-1} + 0.05R$, and $f_m = 35$ Hz. The choice of other parameters is given following equation (2).

Table 6 lists the fault parameters we have used in the application of the FSM. A sketch of the fault geometry may be found in Beresnev and Atkinson (1997). The calculations were performed at points above the upper edge of the fault

Table 6

Parameters of the Fault Used in the Synthesis of Ground Motion using Finite-Source Model of Beresnev and Atkinson (1997)

Event	Strike*	Dip*	Depth to the upper edge of the fault	Length along strike [†] /Number of subfaults along strike [‡]	Width along dip [†] /Number of subfaults along dip [‡]	Subfault where the rupture initiates
Uttarkashi, 19 Oct. 1991, M_w 6.8	317°	14°	10 km	28 km/5	22.5 km/4	(3,3)
Jabalpur, 21 May 1997, M_w 5.8	63°	70°	33 km	7.9 km/4	7.9 km/4	(3,3)
Chamoli, 28 Mar. 1999, M_w 6.5	280°	7°	20 km	20 km/5	16 km/4	(3,3)
Bhuj, 26 Jan. 2001 M_w 7.6	66°	64°	10 km	44 km/5	33 km/4	(3,4)
Bhuj, 28 Jan. 2001 M_w 5.7	78°	51°	12 km	7.5 km/4	7.5 km/4	(3,3)

*Strike and dip of the fault from Harvard CMT catalog.

[†]Except for the Bhuj earthquake (M_w 7.6), the rupture area has been estimated from the relation $\log A = M_w - 4$ (A in km^2) (Singh *et al.*, 1980) and L and W has been arbitrarily assigned. For Bhuj earthquake, L and W are taken from the aftershock distribution.

[‡]Number of subfaults along strike and dip is approximately based on the subfault dimension, l , estimated from the relation $\log l = 0.4 M_w - 2.0$. However, the total number of subfaults is always taken to be ≥ 16 .

and along a line bisecting the length of the fault and traversing toward the southern quadrant. We use random normally distributed fault slip for all events except for the Bhuj mainshock. For this event we also simulate ground motions by specifying a slip distribution, based on the teleseismic body-wave inversion. Peak ground motion at each point is calculated from an average of 15 simulations. The simulated acceleration time histories are high-pass filtered at 0.1 Hz and integrated to obtain velocity traces. For the Bhuj mainshock, we also present contours of A_{\max} and V_{\max} in the near-source region. Note that FSM calculations can't be performed at distances less than the depth of the upper edge of the fault.

We emphasize that our predictions are valid for hard sites since the data at $R > 200$ km were recorded by permanent broadband stations located on rock sites. The two horizontal components are treated independently.

Chamoli Earthquake of 28 March 1999 (M_w 6.5)

The Chamoli earthquake is the only event, listed in Table 1, that was recorded by accelerographs in the distance range of $22 < R < 95$ km and by broadband seismographs from about 820 to 2440 km (Table 5). Note that the data from *known* soft sites (Roorkee, Panipat, CSIR, IHC, and CPCB) are not plotted in Figure 6. However, site characteristics of the accelerographic stations included in the figure are not known.

As shown in Figure 6, the computed ground motions with $\Delta\sigma = 150$ bars are in accord with the observed A_{\max} and V_{\max} at $R > 820$ km and at Ridge Observatory, Delhi ($R = 293$ km). This $\Delta\sigma$ also explains reasonably well the observed data at $R < 130$ km. We can interpret this result in two ways: (1) $Q(f) = 508f^{0.48}$ is adequate for regional distances. The same $\Delta\sigma$ of 150 bars explains observed data at far and near-source distances because the site effects are roughly similar at all stations. (2) The Q at regional distances is actually higher than $Q(f) = 508f^{0.48}$. If so, a $\Delta\sigma$ smaller than 150 bars will be required to fit the data at $R > 290$ km (see Fig. 5). In this case, the larger stress drop of 150 bars

is required to explain the near-source data because the seismic waves at these accelerometric sites are amplified.

The computations with strength factor of 1.4 for A_{\max} and 1.7 for V_{\max} match the respective predicted curves for the AFSM with $\Delta\sigma = 150$ bars up to distance of about 500 km. For reason mentioned earlier, the predicted values at larger distances using FSM are smaller than those from AFTSM for this and the other five earthquakes considered below. Henceforth, the reported *sfact* will refer to that value whose predictions agree with those from the AFTM in the far field at $R < 500$ km.

Uttarkashi Earthquake of 19 October 1991 (M_w 6.8)

The Uttarkashi earthquake gave rise to strong motion recordings from a distance range of about 10–150 km (Yu *et al.*, 1995). The rupture history of this earthquake was studied by Cotton *et al.* (1996). Because the earthquake occurred before the installation of broadband network, there are no recordings at larger distances. Figure 7 shows that the A_{\max} and V_{\max} data can be explained by $\Delta\sigma = 75$ and 40 bars, respectively. It should be kept in mind that the recordings of this earthquake may have been affected by site effects. In a later section, we will discuss the possible causes of the difference between $\Delta\sigma$ required to explain A_{\max} and V_{\max} . The FSM requires *sfact* = 1.0 to roughly match the predicted curves for the AFSM in the far field up to $R < 500$ km.

Jabalpur Earthquake of 21 May 1997 (M_w 5.8) and Bhuj Aftershock of 28 January 2001 (M_w 5.7)

The A_{\max} and V_{\max} data of these two earthquakes, of similar magnitude, are shown in Figures 8 and 9. It is clear that the peak ground motions during the Jabalpur earthquake were greater than those from the Bhuj aftershock. The A_{\max} and V_{\max} data for the Jabalpur event can be explained by $\Delta\sigma = 400$ and 200 bars, respectively, while the corresponding values for Bhuj aftershock are 50 and 35 bars. These two events are associated with the largest $\Delta\sigma$ (Jabalpur) and the smallest $\Delta\sigma$ (Bhuj aftershock) of the events analyzed in this

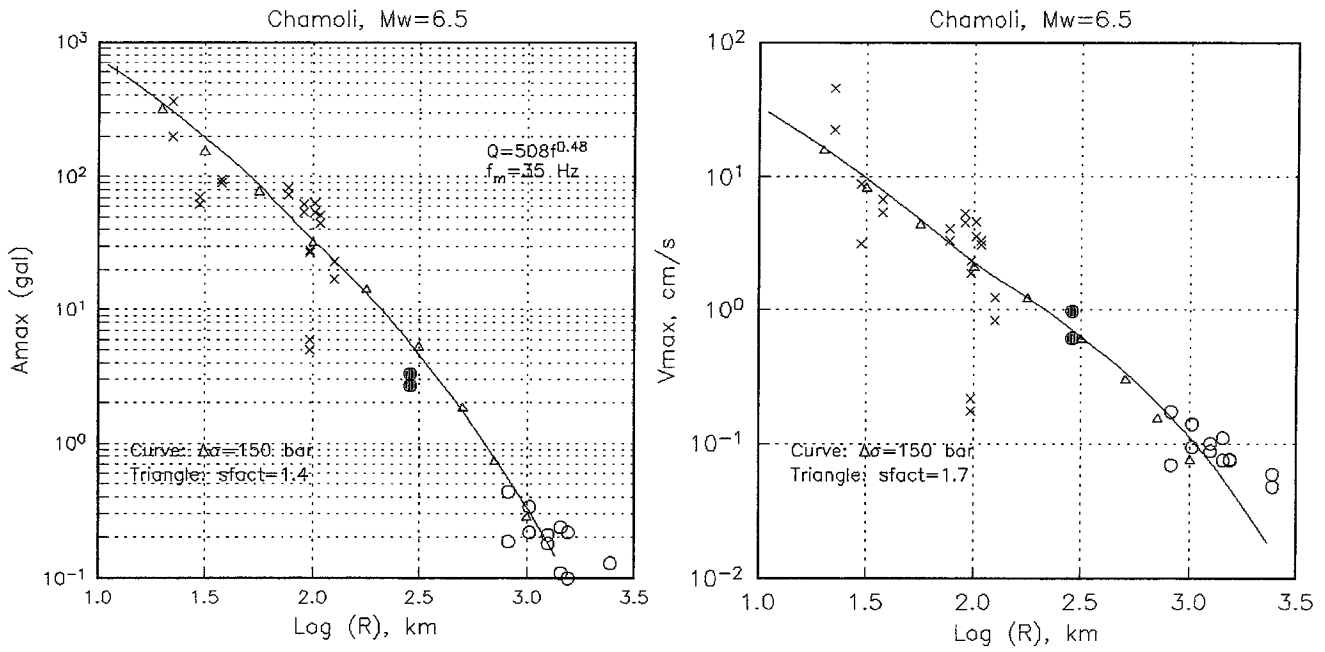


Figure 6. Horizontal component of Amax and Vmax as a function of closest distance, R , from the fault during the Chamoli earthquake. Cross, data from analog accelerogram digitized at 50 Hz; circle, data at 20 Hz. Predicted ground motion from the two finite-source models, with $Q = 508f^{0.48}$, $f_m = 35$ Hz are also shown. Curve, approximate finite-source model (AFSM) with $\Delta\sigma = 150$ bars; triangle, finite-source model (FSM) with $sfact = 1.4$ for Amax and 1.7 for Vmax.

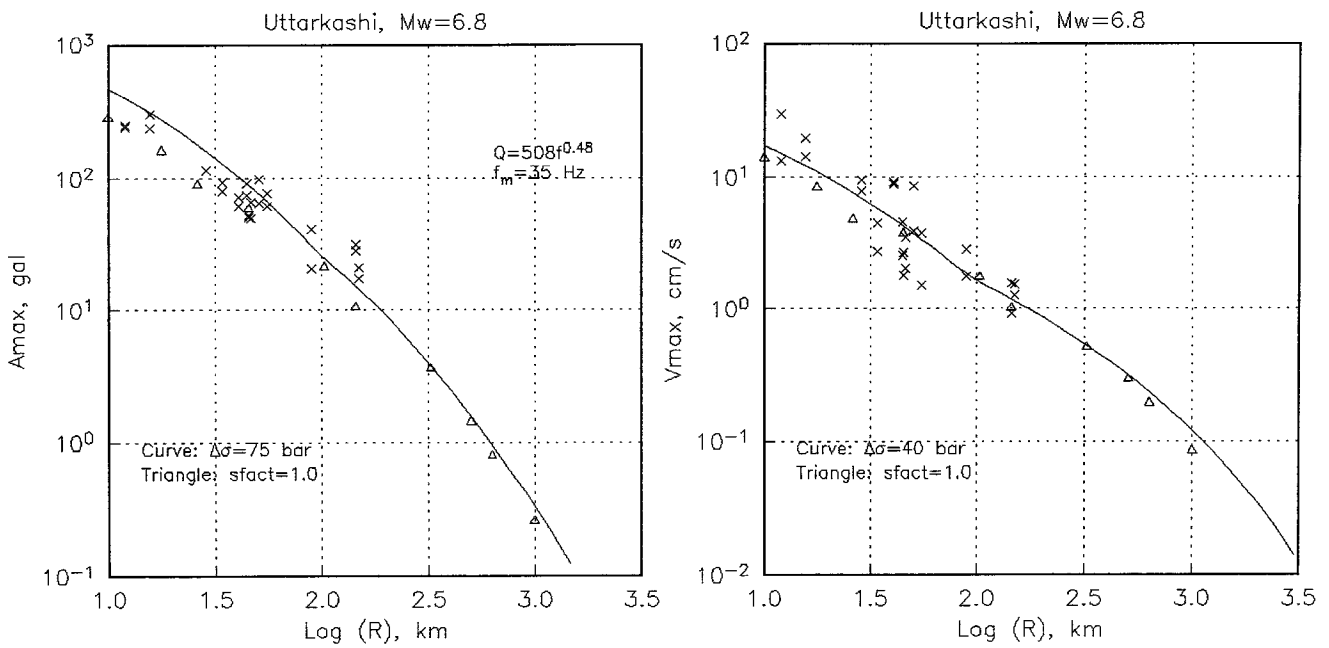


Figure 7. Same as Figure 6 but for Uttarkashi earthquake. Cross, data from analog accelerogram digitized at 50 Hz; curve, AFSM with $\Delta\sigma = 75$ bars (Amax) and 40 bars (Vmax); triangle, FSM with $sfact = 1.0$ (both Amax and Vmax).

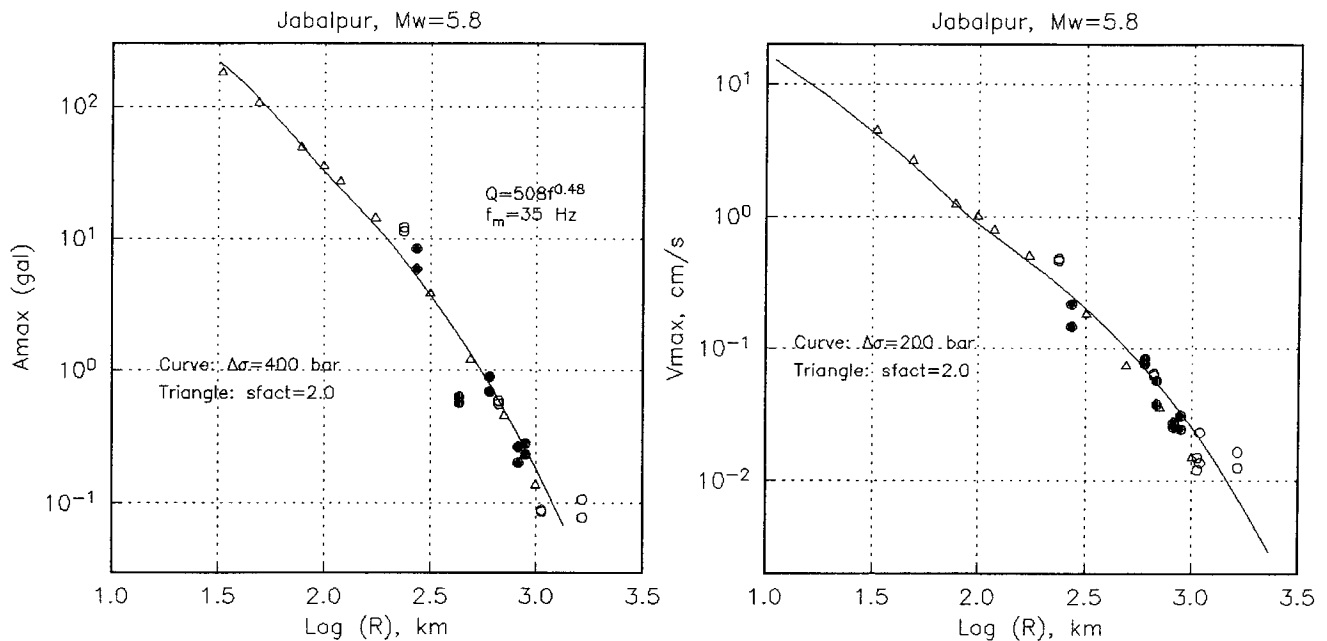


Figure 8. Same as Figure 6 but for Jabalpur earthquake. Dot, data at ≥ 50 Hz; circle, data at 20 Hz; curve, AFSM with $\Delta\sigma = 400$ bars (Amax) and 200 bars (Vmax); triangle, FSM with $s_{fact} = 2.0$ (both Amax and Vmax).

study (see Table 1). We note that the Jabalpur earthquake is also the deepest event in our data set.

The Jabalpur event was previously analyzed by Singh *et al.* (1999), who concluded that Amax data for this earthquake for $R \leq 1000$ km fall between the curves for $\Delta\sigma$ of 200 and 400 bars. They also noted that the recorded Vmax data for $R \leq 1000$ km suggest a smaller $\Delta\sigma$ of 50 to 200 bars. Our results here are in general agreement with those reported by Singh *et al.* (1999).

The strength factors for Jabalpur and the Bhuj aftershock are 2.0 and 1.0, respectively. The predictions from the two models are nearly the same in the near-source region at this magnitude level.

Bhuj Earthquake of 26 January 2001 (M_w 7.6)

As mentioned earlier, on-scale recordings of this earthquake are available at distances $R \geq 565$ km (Fig. 2, Table 2). The observed data are plotted in Figure 10. The predicted Amax and Vmax curves, with $\Delta\sigma = 200$ and 100 bars, respectively, fit the data very well. The predicted Amax and Vmax values on hard sites at $R = 240$ km, the distance to the city Ahmedabad, which was damaged during the Bhuj earthquake, are about 30 Gal and 4 cm/sec. The peak acceleration on the ground floor of a 10-floor building in Ahmedabad was measured at 100 Gal. The larger recorded Amax may have been due to the soft subsoil in Ahmedabad and building-soil interaction. There is also, as noted earlier, some doubt about the performance of the accelerograph.

The predicted Amax and Vmax values at distances of $R < 30$ km exceed 0.5 g and 30 cm/sec. No field evidence of surface rupture was found. Aftershocks were mostly con-

finned to depths greater than 10 km (see later section). This suggests that the closest point on the surface to the rupture area was ≥ 10 km. At $R = 10$ km, Amax and Vmax are 1.35 g and 60 cm/sec, respectively. While these values appear reasonable for hard rock sites, they should be interpreted with caution. First, these predictions are constrained by data at $R \geq 565$ km and, hence, depend on the parameters chosen in the application of the stochastic method. Second, the rupture model used for the modeling is an approximate one.

We now apply the more appropriate FSM to estimate Amax and Vmax in the near-source region of the Bhuj earthquake. Because of the importance of this earthquake, we discuss in some detail the parameters chosen in the simulation (Table 6). Aftershock studies (e.g., Horton *et al.*, 2001; Mandal *et al.*, 2001; Negishi *et al.*, 2001) are consistent with the nodal plane defined by strike = 66° , dip = 64° , and rake = 60° (Harvard CMT catalog), as the fault plane. Most of the aftershocks were clustered in the depth range of 10 to 30 km. The along-strike length of the aftershock zone was about 40 to 45 km. Waveform analysis suggests that the rupture propagation along the strike was essentially bilateral (Kikuchi and Yamanaka, 2001; Mori, 2001). J. Boatwright (personal comm., 2001) and X. Pérez (personal comm., 2001) report that the source spectrum, retrieved from teleseismic P -wave data, follows almost a perfect ω^2 -source model with a corner frequency of 0.07 Hz. Based on the source information summarized previously, we assume a rectangular rupture area with $L = 44$ km, $W = 33$ km; depth to the top of the fault = 10 km; strike $\phi = 66^\circ$, and dip $\delta = 64^\circ$. We subdivide the fault in 5×4 subfaults. We

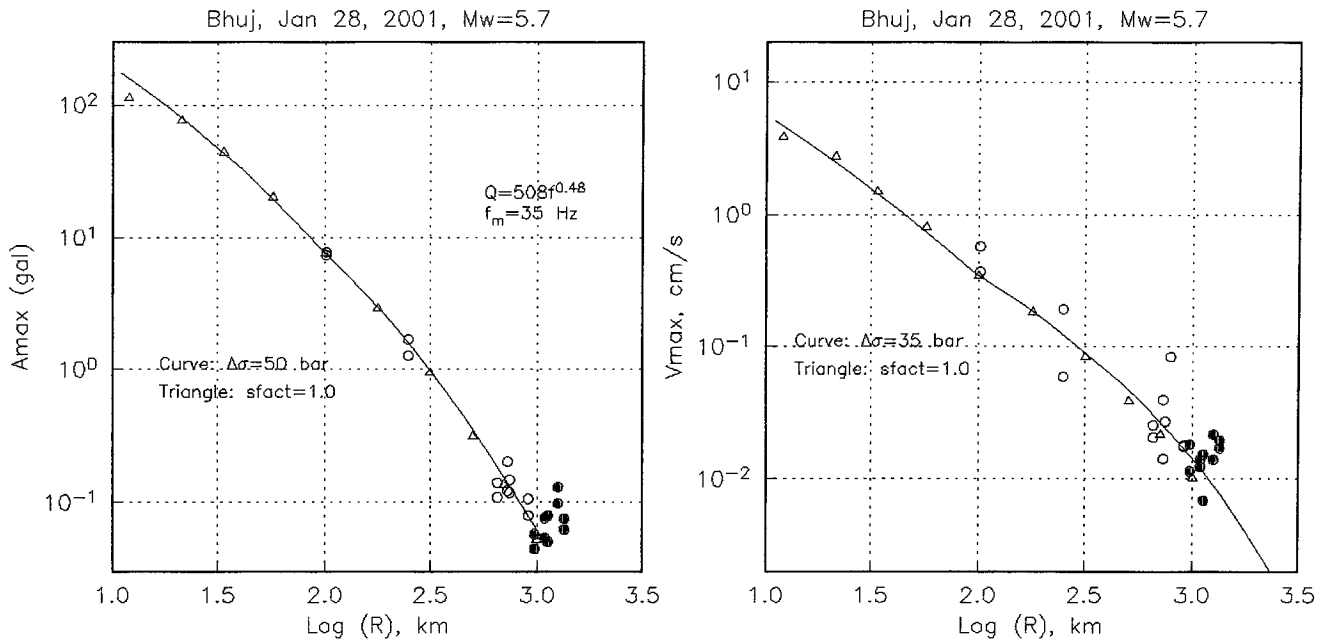


Figure 9. Same as Figure 6 but for the Bhuj aftershock of 28 January 2001. Dot, data at ≥ 50 Hz; circle, data at 20 Hz; curve, AFSM with $\Delta\sigma = 50$ bars (Amax) and 35 bars (Vmax); triangle, FSM with $s_{fact} = 1.0$ (both Amax and Vmax).

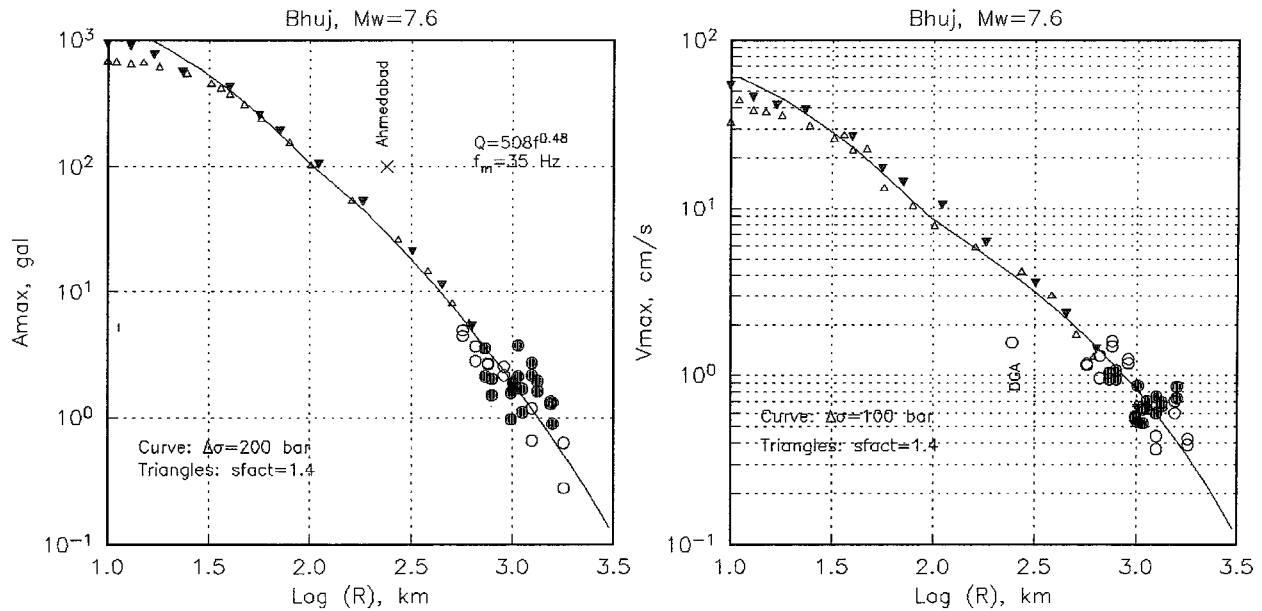


Figure 10. Bhuj mainshock. Dot, data at ≥ 50 Hz; circle, data at 20 Hz; curve, AFSM with $\Delta\sigma = 200$ bars (Amax) and 100 bars (Vmax); triangle, FSM with $s_{fact} = 1.4$ (both Amax and Vmax); open triangle, random slip; solid triangle, prescribed slip. The DGA data provide a lower bound. Amax recorded at Ahmedabad is also indicated.

assume that the rupture started at the center of the bottom edge of the fault (Table 6). All other parameters are the same as those used for the case of the approximate finite-source model. From Figure 10 we note that $s_{fact} = 1.4$ explains the observed Amax and Vmax data in the far field. The predicted values from the two models are nearly equal at $R >$

40 km. The results from several sets of simulations (one sample is shown in Fig. 10) indicate Amax and Vmax values of about 0.8 g and 45 cm/sec above the fault. The contours of Amax and Vmax from another set of simulations are shown in Figure 11 (top frames). The calculations were made at grid points spaced 0.0025° (~ 250 m). The model

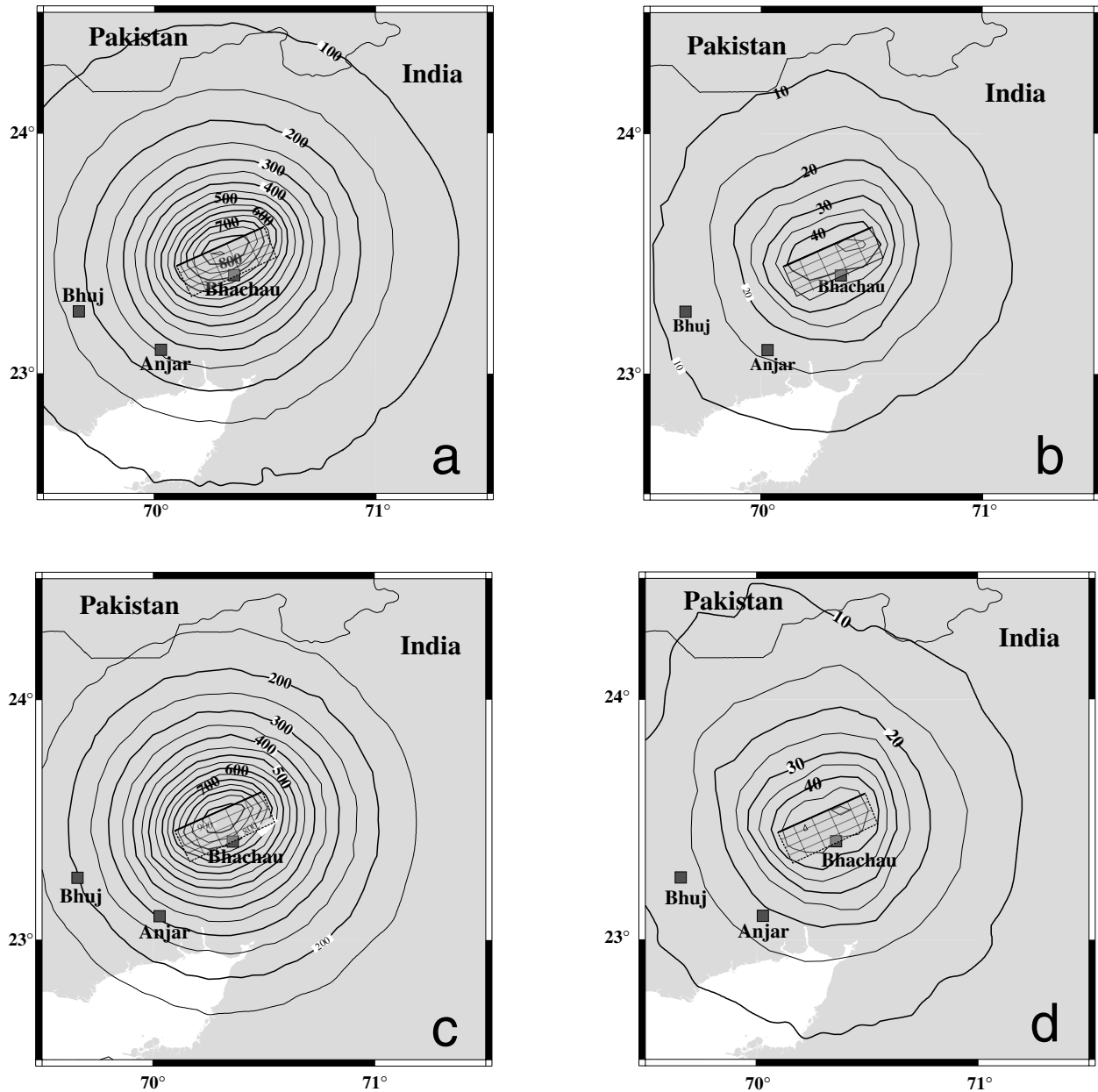


Figure 11. Contours of predicted A_{max} and V_{max} during the Bhuj earthquake based on FSM with $s_{fact} = 1.4$. Rectangle is the horizontal projection of the fault plane. Thick line indicates projection of the top edge of the fault. The fault area is divided in 5×4 subfaults. The rupture initiates in the subfault (3,4) that lies below Bhachau. Table 6 gives the input parameters. Top frames, random normally-distributed slip with standard deviation equal to the mean slip. Bottom frame, prescribed slip (Table 7).

predicts A_{max} of about $0.7 g$ in Bhachau, a town in the epicentral region that was completely destroyed during the earthquake, and $>0.25 g$ and $>0.15 g$ in Anjar and Bhuj, respectively (Fig. 11, top frames), both of which were severely damaged during the earthquake.

We also carried out simulations with a prescribed slip distribution based on the results of teleseismic body-wave inversion (Kikuchi and Yamanaka, 2001; Mori, 2001; Yagi and Kikuchi, 2001). The inversion of Yagi and Kikuchi

(2001) suggests a larger rupture area than the aftershock area and rupture propagation toward the west. Source time functions of the earthquake, obtained from a deconvolution of the mainshock with the aftershock of 28 January 2001 recorded at teleseismic and regional distances, do not reveal a pronounced directivity. The slip distribution and the fault area reported by Kikuchi and Yamanaka (2001) and Mori (2001) are in better agreement with these observations. In our simulations we discretized the slip distribution of Mori

(2001). Table 7 gives the slip in each subfault. A large constant slip of 10.4 m is distributed over an area of $8.8 \times 16.5 \text{ km}^2$. The total seismic moment, assuming a rigidity of $\mu = 4.5 \times 10^{11} \text{ dyne/cm}^2$, is $3.5 \times 10^{27} \text{ dyne-cm}$. The computation assumes $s_{fact} = 1.4$. The rupture initiates in subfault (3,4), which is located just below Bhachau. Figure 11C and D show contours of Amax and Vmax. As a consequence of concentrated slip over a relatively small area, the predicted ground motions in the near-source region and at distances up to 350 km are now larger than in the case of randomly generated slip (Figs. 10 and 11). The Amax and Vmax values above the upper edge of the fault reach 0.95 g and 55 cm/sec. The estimated Amax values are 10%–15% higher in Bhachau, Anjar, and Bhuj than in the case of the random slip.

The Bhuj earthquake produced seismoscope traces on 13 Structural Response Recorders (SSR), operated by University of Roorkee in the Kachchh region (Chandra *et al.*, 2002). These units consist of two sets of three oscillators (periods 0.4, 0.75, and 1.25 sec) with 5% and 10% of critical damping. The site characteristics of the recording stations are not known. From the maximum deflection of the traces, Chandra *et al.* (2002) provide an estimate of Amax at these sites. The estimates are based on generic site classification and the resulting expected shape of the response spectra. These estimated values, along with our predicted values (corresponding to randomly generated slip on the fault), are listed in Table 8. We note that Amax estimated from SSR at rock and alluvium sites are, on an average, 1.8 and 2.4 times greater than our predictions, which are for hard sites. In view of the uncertainties involved, the comparison is very encouraging. A detailed study of near-surface subsoil characteristics at SSR sites may prove useful in constraining input ground motion during the earthquake and may provide a check on our results.

Comparison with Some Other Attenuation Relations

In this section we compare our results for the Indian shield region with those developed by Atkinson and Boore (1995) for the eastern North America. We also compare our predictions for the Himalayan arc with those obtained by Parvez *et al.* (2001) for the western Himalayas. An exhaus-

tive list of attenuation relations developed for India can be found in Parvez *et al.* (2001).

The attenuation relations of Atkinson and Boore (1995) are constrained by data in the magnitude range $4.0 \leq M_w \leq 6.8$, while those by Parvez *et al.* (2001) are based on two events (M_w 5.5 and 6.8), one which is the Uttarkashi earthquake of 1991 (Table 1). To minimize the uncertainties that may arise from large extrapolation, we compare the predictions for an M_w 7 earthquake. Our computations are based on AFSM. Figure 12 shows predicted curves corresponding to the stress parameters of the three Indian shield earthquakes and the two Himalayan arc events (Table 1). It is clear that the shapes of attenuation curves for the ENA and Indian shield differ (Fig. 12, top frames). This reflects $G(R) = R^{0.0}$ assumed by Atkinson and Boore (1995) in the distance range $70 \leq R \leq 130 \text{ km}$ for the ENA. The Amax curve for the ENA region is close to the curve for the Indian shield region with $\Delta\sigma = 200 \text{ bar}$. Vmax for ENA, on the other hand, lies between the curves for $\Delta\sigma = 35$ and 75 bars.

For the western Himalayas, the shapes of the attenuation curves of Parvez *et al.* (2001) differ from those of the present study. The attenuation rate is smaller for $R > 80 \text{ km}$ in Parvez *et al.* compared with our study. We note, however, that there were only two recordings at $R > 100 \text{ km}$ in the data set used by Parvez *et al.* Hence, the predictions of Parvez *et al.* for $R > 100 \text{ km}$ are not well constrained by the data. For $R < 100 \text{ km}$, the predictions by Parvez *et al.* are close to our results for the Uttarkashi earthquake. This is partly due to the fact that one of the two earthquakes used in the analysis of Parvez *et al.* is the Uttarkashi event.

Discussion and Conclusions

Table 1 lists the estimated values of $\Delta\sigma$ and s_{fact} of each earthquake studied here. The peak ground motions computed using these parameters and the stochastic models, outlined previously, are in accordance with the observed data on hard sites. Near-source recordings are available for the Chamoli and Uttarkashi earthquakes only. For other events the data are from regional distances, mostly from $R > 500 \text{ km}$, with a few recordings in the 230–300 km range. At these regional distances, the peak ground motion is controlled by Q as well as $\Delta\sigma$ and s_{fact} . The fact that the same

Table 7
Prescribed Slip on Subfaults* of Bhuj Earthquake of 26 January 2001†

(1,1) [‡] , 3.5 m [§]	(1,2), 5.8 m	(1,3), 5.8 m	(1,4), 5.8 m	(1,5), 3.5 m
(2,1), 3.5 m	(2,2), 5.8 m	(2,3), 10.4 m	(2,4), 5.8 m	(2,5), 3.5 m
(3,1), 3.5 m	(3,2), 5.8 m	(3,3), 10.4 m	(3,4), 5.8 m	(3,5), 3.5 m
(4,1), 3.8 m	(4,2), 5.8 m	(4,3), 5.8 m	(4,4), 5.8 m	(4,5), 3.5 m

*Five along strike and four along the dip.

†Modified from Mori *et al.* (2001).

‡Subfault.

§Slip.

Table 8
Comparison of Estimated Amax from Structural Response Recorders* and Predicted Amax
in This Study During the Bhuj Mainshock

Location	Site Class for SSR	Distance [†] , km	Estimated Amax from SSR, Gal	Predicted Amax at Hard Site, Gal	Estimated/Predicted Amax
Anjar	Rock	30	547	250	2.19
Naliya	Rock	147	168	66	2.55
Khambhaliya	Rock	150	50	68	0.76
Jamodhpur	Rock	166	118	52	2.27
Junagarh	Rock	216	49	32	1.53
Amreli	Rock	225	51	30	1.70
Kandla	Alluvium	50	333	280	1.19
Niruna	Alluvium	97	379	100	3.79
Dwarka	Alluvium	188	29	49	0.59
Porbandar	Alluvium	207	144	36	4.00
Ahmedabad	Alluvium	238	134	29	4.62
Cambay	Alluvium	266	24	22	1.09
Anand	Alluvium	288	36	21	1.71

*Chandra *et al.*, 2002.

[†]Approximate closest distance to the fault.

$\Delta\sigma$ (and, indirectly, *sfact*) explain both the regional and the near-source data for the Chamoli earthquake suggests that $Q = 508f^{0.48}$ is reasonable for the Indian-shield as well as the Himalayan-arc earthquakes. Because of tradeoff between Q and $\Delta\sigma$ at regional distances and unknown site characteristics of near-source stations, it is possible, however, that Q , in fact, is greater. If so, then a smaller $\Delta\sigma$ (and, hence, *sfact*) can explain the regional hard-rock data. This smaller $\Delta\sigma$ and *sfact* will underestimate the observed near-source data, which in this case can be explained by amplification of seismic waves at these sites. In spite of these uncertainties, the stress parameters and strength factors listed in Table 1 provide important, albeit preliminary, information for predicting ground motions from future earthquakes in India. The stress parameter needed to explain Amax data is about twice that required for the Vmax data, the only exception being the Chamoli earthquake (Table 1). The different $\Delta\sigma$ values required for Amax and Vmax may result from (1) the inadequacy of the simple ω^2 -source model assumed in this study in the application of the approximate finite-source model, (2) a consequence of the attenuation function, even if the sources follow the ω^2 model (e.g., Luco, 1985), or (3) a more pronounced site effect at frequencies associated with Amax than with Vmax. We cannot identify the cause of the difference, although we note that the $\Delta\sigma$ values for Amax and Vmax differ for the Bhuj mainshock even though the source almost perfectly conform to the ω^2 model. Curiously, in cases when $\Delta\sigma$ value for Amax is twice the value for Vmax, the value *sfact* is about the same (Table 1).

There is some evidence that the stress parameter, $\Delta\sigma$, (and strength factor, *sfact*) for predicting Amax from shield events may be a function of depth, increasing from ~ 50 bars (*sfact* = 1.0) at 10 km to ~ 400 bars (*sfact* = 2.0) at 36 km. The $\Delta\sigma$ value for estimating Vmax may be roughly half the corresponding value for Amax, while the *sfact* may be the

same. The Chamoli and Uttarkashi earthquakes suggest that $\Delta\sigma$ of 150 bars may provide a reasonably conservative estimation of both Amax and Vmax for Himalayan arc earthquakes. The corresponding *sfact* values for Amax and Vmax are 1.4 and 1.7, respectively. We reiterate that these results depend on the assumption of the source model, and on parameters that have been fixed in these computations, the important ones being Q , the form of the geometrical spreading term $G(R)$, and the effective duration of the ground motion. There is a lack of relevant studies on these topics in India. For the stochastic method to provide reliable estimation of ground motion in India, vigorous research on these and related topics is urgently needed.

Figures 10 and 11 provide our estimations of Amax and Vmax values at hard sites during the Bhuj mainshock. These estimations are based on the two models that account for the finiteness of the fault. The predicted Amax and Vmax values from both models exceed 0.5 *g* and 30 cm/sec, respectively, at distances of less than 30 km from the fault. The Amax and Vmax values above the fault are estimated as 0.80–95 *g* and 40–55 cm/sec. Our calculations suggest that the earthquake generated Amax values in excess of 10% *g* to distances of about 100 km even on hard rocks. Field observations have shown extensive liquefaction and lateral spreading in the epicentral region. Since our predictions are for hard sites (assuming no nonlinear behavior of the subsoil), it is not straightforward to check the validity of these predictions from the field observations.

Acknowledgments

This study would not have been possible without the availability of the data collected by the following institutions of India: India Meteorological Department/Department of Science and Technology; DEQ, University of Roorkee; National Geophysical Research Institute; Geological Survey

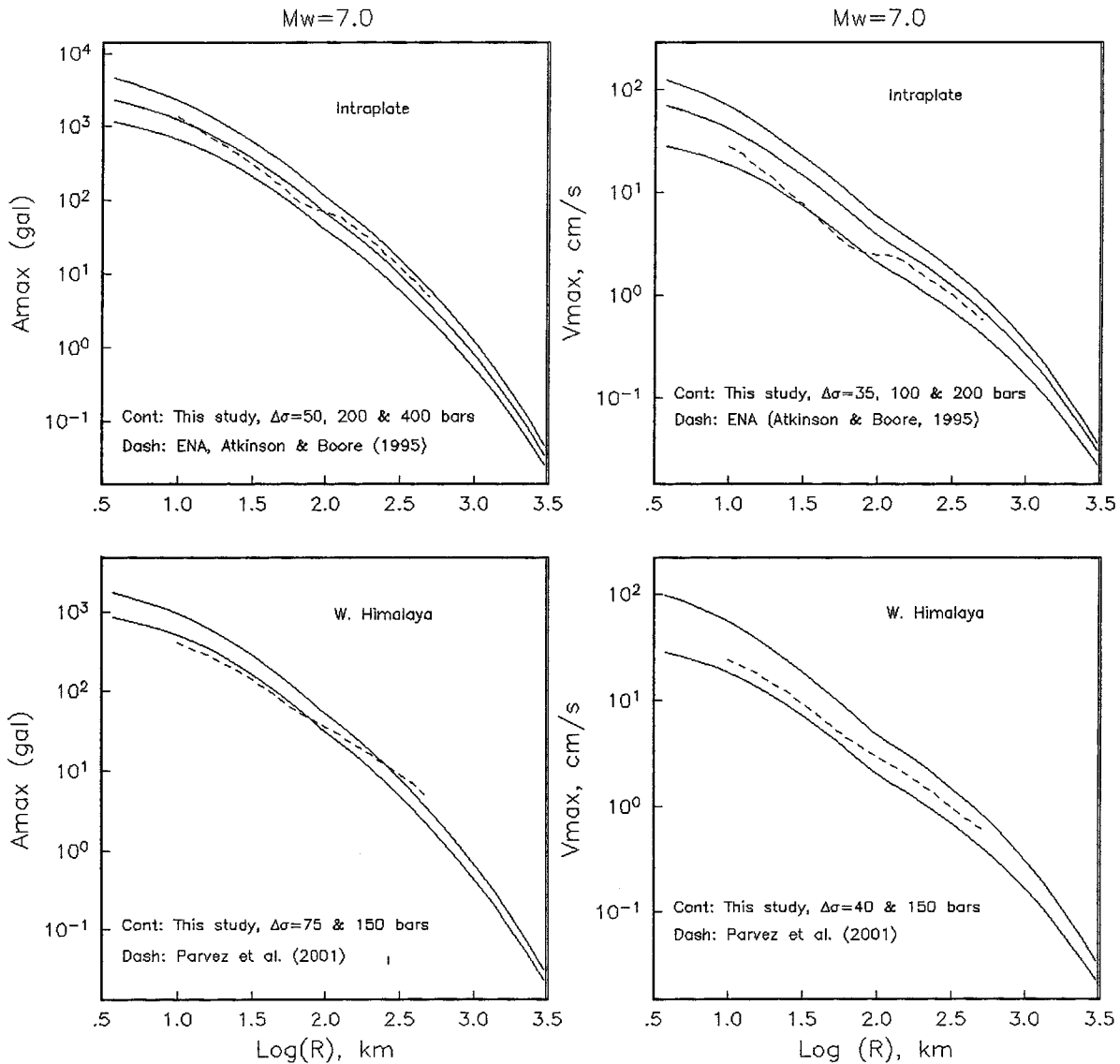


Figure 12. Comparison of predicted peak ground motions. M_w 7.0. Continuous curves are from this study, corresponding to the stress parameters listed in Table 1 and computed using AFSM. Top frames, Indian shield and eastern North America regions (dashed curve, Atkinson and Boore, 1995). Bottom frames, western Himalayas (dashed curves from Parvez *et al.*, 2001).

of India; Gujrat Engineering Research Institute; Osmania University; Indian Institute of Geomagnetism, Mumbai; Wadia Institute of Himalyan Geology; Centre for Earth Science Studies; National Institute of Rock Mechanics. The authors are grateful to the Director General of India Meteorological Department for permission to use the data and for publishing the article. They express their gratitude to the authorities of the other institutions for providing the data. Access to information and preprints, provided by many scientists worldwide, was indispensable to our study. We especially thank Roger Bilham, Jack Boatwright, Paul Bodin, Joan Gomberg, Sudhir K. Jain, Jim Mori, D.K. Paul, Xyoli Pérez, and T. Sato for sharing information and/or preprints prior to publication. Igor Beresnev patiently explained the FINSIM program to us. Fruitful discussions with Kailash Khattri and Harsh Gupta are acknowledged. We thank Secretary D.S.T. for his continuous support and guidance. The manuscript was revised by Paul Bodin, Joan Gomberg, and Roger Bilham. The research was partially supported by UNAM, DGAPA Projects IN111601.

References

- Anderson, J. G., and S. E. Hough (1984). A model for the shape of the Fourier amplitude spectrum of acceleration at high frequencies, *Bull. Seism. Soc. Am.* **74**, 1969–1993.
- Atkinson, G. M., and D. M. Boore (1995). Ground motion relations for eastern North America, *Bull. Seism. Soc. Am.* **85**, 17–30.
- Atkinson, G. M., and D. M. Boore (1998). Some comparisons between recent ground motion relations, *Seism. Res. Lett.* **68**, 24–40.
- Beresnev, I. A., and G. Atkinson (1997). Modelling finite fault radiation from the ω^p spectrum, *Bull. Seism. Soc. Am.* **87**, 67–84.
- Beresnev, I. A., and G. Atkinson (1998). FINSIM-a Fortran program for simulating stochastic acceleration time histories from finite faults, *Seism. Res. Lett.* **69**, 27–32.
- Beresnev, I. A., and G. Atkinson (1999). Generic finite-fault model for ground motion prediction in eastern North America, *Bull. Seism. Soc. Am.* **89**, 608–625.

- Beresnev, I. A., and G. Atkinson (2001). Subevent structure of large earthquakes—a ground-motion perspective, *Geophys. Res. Lett.* **28**, 53–56.
- Beresnev, I., and G. Atkinson (2002). Source parameters of earthquakes in eastern and western North America based on finite-fault modelling, *Bull. Seism. Soc. Am.* **92**, 695–710.
- Bhattacharya, S. N., A. K. Ghose, G. Suresh, P. R. Baidya, and R. C. Saxena (1997). Source parameters of Jabalpur earthquake of 22 May 1997, *Curr. Sci.* **73**, 855–863.
- Bilham, R., V. K. Gaur, and P. Molnar (2001). Himalayan seismic hazard, *Science* **293**, 1442–1444.
- Boore, D. M. (1983). Stochastic simulation of high-frequency ground motions based on seismological models of radiated spectra, *Bull. Seism. Soc. Am.* **73**, 1865–1884.
- Boore, D. M., and G. M. Atkinson (1987). Stochastic prediction of ground motion and spectral response parameters at hard-rock sites in eastern North America, *Bull. Seism. Soc. Am.* **77**, 440–467.
- Brune, J. N. (1970). Tectonic stress and the spectra of seismic shear waves from earthquakes, *J. Geophys. Res.* **75**, 4997–5009.
- Cartwright, D. E., and M. E. Longuet-Higgins (1956). The statistical distribution of maxima of a random function, *Proc. R. Soc. London, Ser. A.* **237**, 212–232.
- Chandra, B., S. K. Thakkar, S. Basu, A. Kumar, M. Shrikhande, J. Das, P. Agarwal, and M. K. Bansal (2002). Strong motion records, *Earthquake Spectra*, submitted.
- Cotton, F., M. Campillo, A. Deschamps, and B. K. Rastogi (1996). Rupture history and seismotectonics of the 1991 Uttarkashi earthquake, *Tectonophysics* **258**, 35–51.
- Hanks, T. C. (1982). f_{max} , *Bull. Seism. Soc. Am.* **72**, 1867–1879.
- Hanks, T. C., and R. K. McGuire (1981). The character of high-frequency strong ground motion, *Bull. Seism. Soc. Am.* **71**, 2071–2095.
- Herrmann, R. B. (1985). An extension of random vibration theory estimates of strong ground motion at large distances, *Bull. Seism. Soc. Am.* **75**, 1447–1453.
- Herrmann, R. B., and A. Kijko (1983). Modelling some empirical vertical component L_g relations, *Bull. Seism. Soc. Am.* **73**, 157–171.
- Horton, S., P. Bodin, A. Johnston, G. Patterson, J. Bollwerk, P. Rydelek, A. Raphael, J.-M. Chiu, K. Budhbhatti, and J. Gombert (2001). Bhuj aftershocks recorded by the MAEC/ISTAR temporary seismic network, Abstract, *Intern. Conf. on Seismic Hazard with Particular Reference to Bhuj Earthquake of January 26, 2001*, New Delhi, 3–6 October, 102–103.
- Khattri, K. N. (1999). An evaluation of earthquakes hazard and risk in northern India, *Himalayan Geol.* **20**, 1–46.
- Kikuchi, M., and Y. Yamanaka (2001). Western India earthquake, <http://www.weic.u-tokyo.ac.jp/index-e.html>.
- Luco, J. E. (1985). On strong ground motion estimates based on models of the radiated spectrum, *Bull. Seism. Soc. Am.* **75**, 641–649.
- Mandal, P., B. K. Rastogi, H. V. S. Satyanaraya, M. Kousalya, C. Satyamurty, I. P. Raju, and N. Kumar (2001). Characterization of the causative fault system for the 2001 Bhuj earthquake, Abstract, *Intern. Conf. on Seismic Hazard with Particular Reference to Bhuj Earthquake of January 26, 2001*, New Delhi, 3–6 October, 109–112.
- Mori, J. (2001). Slip distribution of mainshock, in *A comprehensive survey of the 26 January 2001 earthquake (Mw7.7) in the state of Gujrat, India*, T. Sato (Editor), Report by the research team supported by the grant-in-aid for specially promoted research provided by MEXT of Japan in the fiscal year of 2000, 41–45.
- Negishi, H., J. Mori, T. Sato, R. P. Singh, and S. Kumar (2001). Aftershocks observations, in *A comprehensive survey of the 26 January 2001 earthquake (Mw7.7) in the state of Gujrat, India*, T. Sato (Editor), Report by the research team supported by the grant-in-aid for specially promoted research provided by MEXT of Japan in the fiscal year of 2000, 33–40.
- Papageorgiou, A. S., and K. Aki (1983). A specific barrier model for the quantitative description of inhomogeneous faulting and the prediction of strong motion. I. Description of the model, *Bull. Seism. Soc. Am.* **73**, 693–722.
- Parvez, I. A., A. A. Gusev, G. Panza, and A. G. Petukhin (2001). Preliminary determination of the interdependence among strong-motion amplitude, earthquake magnitude and hypocentral distance for the Himalayan region, *Geophys. J. Int.* **144**, 577–596.
- Singh, S. K., R. Apsel, J. Fried, and J. N. Brune (1982). Spectral attenuation of SH-wave along the Imperial fault, *Bull. Seism. Soc. Am.* **72**, 2003–2016.
- Singh, S. K., E. Bazan, and L. Esteva (1980). Expected earthquake magnitude from a fault, *Bull. Seism. Soc. Am.* **73**, 693–722.
- Singh, S. K., M. Ordaz, J. G. Anderson, M. Rodriguez, R. Quaaas, E. Mena, M. Ottaviani, and D. Almora (1989). Analysis of near-source strong-motion recordings along the Mexican subduction zone, *Bull. Seism. Soc. Am.* **79**, 1697–1717.
- Singh, S. K., W. Mohanty, B. K. Bansal, and G. S. Roonwal (2002). Ground motion in Delhi from future large/great earthquakes in the central seismic gaps of the Himalayan arc, *Bull. Seism. Soc. Am.* **92**, 555–569.
- Singh, S. K., M. Ordaz, R. S. Dattatrayam, and H. K. Gupta (1999). A spectral analysis of the May 21, 1997, Jabalpur, India earthquake (Mw = 5.8) and estimation of ground motion from future earthquakes in the Indian shield region, *Bull. Seism. Soc. Am.* **89**, 1620–1630.
- Yagi, Y., and M. Kikuchi (2001). Western India earthquake, <http://www.weic.u-tokyo.ac.jp/index-e.html>.
- Yu, G., K. N. Khattri, J. G. Anderson, J. N. Brune, and Y. Zeng (1995). Strong ground motion from the Uttarkashi, Himalaya, India, earthquake: comparison of observations with synthetics using the composite source model, *Bull. Seism. Soc. Am.* **85**, 31–50.

Instituto de Geofísica UNAM
Ciudad Universitaria
04510 México, DF, México
krishna@ollin.igeofcu.unam.mx
(S.K.S., J.F.P.)

Department of Science and Technology
Government of India
New Mehrauli Road
New Delhi, 110016, India
(B.K.B.)

India Meteorological Department
Lodhi Road
New Delhi, 110003, India
(S.N.B., R.S.D., G.S.)

Instituto de Ingeniería, UNAM
Ciudad Universitaria
04510 México, DF, México
(M.O.)

Wadia Institute of Himalayan Geology
33 General Mahadeo Singh Road
Dehradun, 248001, India
(K.)

United States Geological Survey
Pasadena, California 91106
(S.E.H.)